Hydrodynamic-flow-driven wetting in thin film polymer blends: Growth kinetics and morphology

Howard Wang and Russell J. Composto
Department of Materials Science and Engineering and Laboratory for Research on the Structure of Matter, University of Pennsylvania, Philadelphia, Pennsylvania 19104-6272
(Received 9 August 1999)

A thin film of deuterated poly(methyl methacrylate) (*A*) and poly(styrene-*ran*-acrylonitrile) at the critical composition is annealed in the two phase region to induce simultaneous phase separation and wetting of the *A*-rich phase at the surface. Using forward recoil spectrometry, the wetting layer thickness is found to grow linearly with time at 185 °C and 190 °C. After selective etching of *A*, atomic force microscopy reveals a depletion layer having a bicontinuous, phase separated morphology. The *A*-rich tubes in this layer provide a pathway for rapid transport of the wetting phase from the bulk to the surface via hydrodynamic flow. Taken together, fast wetting layer growth t^1 and connectivity between the wetting layer and bulk provide unambiguous support for hydrodynamic-flow-driven wetting in thin film polymer blends.

PACS number(s): 36.20.−r, 64.60.Ht, 68.10.−m

I. INTRODUCTION

Wetting plays an important role in diverse applications ranging from insecticide sprays to detergency. This interest, in part, has motivated a great deal of fundamental research involving the spreading (wetting) of a liquid on a solid surface [1,2]. Polymer blends are of great commercial importance and therefore their thermodynamic and phase separation behavior have been widely studied [3]. In the field of polymers, phase separation and wetting in two-component polymer blends *AB* confined to a thin film is a topic of great recent interest [4–6,10]. Here the phase separation of *A*-rich and *B*-rich domains is modified by confinement resulting in a variety of equilibrium morphologies, which depend on the wetting behavior of the *A*-rich and *B*-rich domains. For example, if the *A*-rich phase prefers both surfaces and the temperature is above the wetting temperature, the *B*-rich phase will be encapsulated by the *A*-rich phases resulting in a trilayer structure.

In coatings where the upper and lower surfaces are air and solid, respectively, lateral phase separation and/or capillary fluctuations can induce surface roughening. Before one can control the final morphology, experimental studies of wetting, phase separation and their interdependence are needed. In those of wetting from a binary system, a wetting layer can grow by either diffusion of the surface preferred component or by hydrodynamic flow of this component through channels in the nonwet layer. For both mechanisms the wetting layer thickness grows as a power-law $l \propto t^{\alpha}$, where α is 1/3 or less for diffusion limited growth [4-6] and close to 1 or higher for hydrodynamic flow [5,7–9]. The particular mechanism will depend on several factors including wettability, composition, viscosity, confinement, and degree of quenching. To date, experimental and theoretical studies have mainly focused on diffusion limited growth in critical blends [4–6,10], whereas unambiguous experimental evidence for hydrodynamic-flow-driven wetting in polymers is still lacking. In this paper, we will present, both signatures of hydrodynamic-flow-driven wetting, namely, t^1 power law wetting layer growth and a bicontinuous near-surface morphology.

Upon quenching into the unstable regime, a thick film of a critical mixture can display an oscillatory concentration profile perpendicular to the surface [10], denoted as surface directed spinodal decomposition. Using a critical mixture of hydrogenated and deuterated poly(ethylene propylene) (PEP and dPEP), Krausch *et al.* [4] observed that the dPEP surface layer grew as $t^{1/3}$, consistent with growth by diffusion of dPEP through a continuous PEP-rich depletion layer. For an off-critical composition rich in the wetting component, the dPEP-rich phase grew as around t^1 at late times [5]. This fast growth mechanism was attributed to the transport of dPEP by hydrodynamic flow through perforations in the PEP-rich depletion layer towards the surface domain. By following the composition profile and surface roughness, Jandt *et al.* [11] demonstrated that phase separating mixtures display surface roughening, which was attributed to either hydrodynamic flow of the wetting phase or coarsening of the underlying nonwetting phase. Although these results are provoking, unambiguous evidence for hydrodynamic flow requires observation of both a fast wetting layer growth rate and a bicontinuous morphology in the depletion layer.

In part because of their low viscosity, small molecule and oligomeric systems typically display hydrodynamic-flow-driven wetting [7–9,12]. Tanaka investigated the interplay between wetting and phase separation in symmetric poly(vinyl methyl ether)/water mixtures and oligomer mixtures confined in one (1D) and two-dimensions (2D) [7]. Using optical microscopy (OM), Tanaka observed that the wetting layer was fed by the hydrodynamic flow of the wetting component from an adjacent bicontinuous network. Also using OM, Guenoun *et al.* [12] studied the phase separation of cyclohexane and methanol near a wall. Due to its limited spatial resolution, OM was unable to follow the early stage of wetting. Wiltzius *et al.* [9] used light scattering to examine the characteristic length scales for low molecular weight polyisoprene and poly(ethylene-propylene) blends undergoing simultaneous phase separation and wetting. The length scale of the phases parallel to the wall was measured rather than the wetting layer itself.

By characterizing the depth profile, surface roughness and internal morphology, we have identified four stages of evo-

lution that thin film blends of deuterated poly(methyl methacrylate) (*A*) and a random copolymer poly(styrene-*ran*-acrylonitrile) (*B*) can display during simultaneous wetting and phase separation. Upon annealing in the unstable regime, both the surface and the substrate are rapidly saturated with *A*, the lower surface energy component. During the second stage, the wetting layer thickness increases by hydrodynamic flow of *A* from the adjacent bicontinuous network. After a *A*-rich/*B*-rich/*A*-rich tri-layer forms, the wetting layer begins to thin as *A* flows back into the bulk of the film through *A*-rich channels perforating the *B*-rich internal layer. As shown in a later paper, these lateral features grow as $t^{1/3}$ during this period. Finally, the encapsulated *B*-rich layer ruptures and forms an interconnected network with large features (i.e., >20 μm). As the *B*-rich phase dewets from the *A*-rich phase, the film roughness increases rapidly. The final morphology appears as *B*-rich droplets encapsulated by the *A*-rich phase. In this paper, we focus on the second regime and report wetting layer growth and depletion layer morphology consistent with hydrodynamic-flow-driven wetting.

II. EXPERIMENTS

The polymer components are deuterated poly(methyl methacrylate) (dPMMA, denoted as component *A* in this paper) and a random copolymer of poly(styrene-*ran*-acrylonitrile) (SAN, denoted as component *B*) having an AN content of 33 wt %. The weight average molecular weights and polydispersities of dPMMA and SAN are 90*k* and 1.06, and 124*k* and 2.24, respectively. PMMA(90*k*):SAN blends exhibit a lower critical solution temperature (LCST) behavior with a critical temperature and composition of 170 °C and around 0.5, respectively, whereas the *AB* blend has a lower critical temperature of around 160 °C [13]. One significant advantage of LCST systems is that the initial blend is thermodynamically stable in contrast to systems having upper critical solution temperatures. Consistent substrate surfaces were prepared by first removing the native oxide layer on as-received silicon using a buffered HF solution. A new oxide layer of 18 Å was grown by exposing a hydrogen terminated silicon surface to ultraviolet radiation and ozone [14]. A critical composition, 50:50 by weight, was used for all samples. The *A* and *B* components were dissolved in methyl iso-butyl ketone and spun cast on silicon to produce 495 nm films as measured by ellipsometry. Films were subsequently dried at 120 °C in a vacuum oven for 24 h. After annealing at 185 °C or 190 °C in Argon for 5 min to 2 h, the depth profile of dPMMA was measured by low-energy forward recoil spectrometry (LE-FRES) [15], and the phase morphology by atomic force microscopy (AFM).

In LE-FRES, 1.0 MeV helium ions impinged on the sample at an angle of $+75°$ with respect to the sample normal. Deuterium and hydrogen atoms from the film were elastically scattered and detected by a solid-state detector located at $-75°$. A 3.0 μm Mylar stopper foil covered the detector and prevented forward scattered He ions from masking the D and H signals. The He energy and stopper foil thickness were chosen to optimize the surface depth resolution, which has a full width half maximum (FWHM) value of 160 Å [16]. The depth profile was averaged over a lateral area of 3 mm^2, the size of the He beam on target. The LE-FRES spectra (5 μC) were produced by combining 1 μC doses on fresh areas.

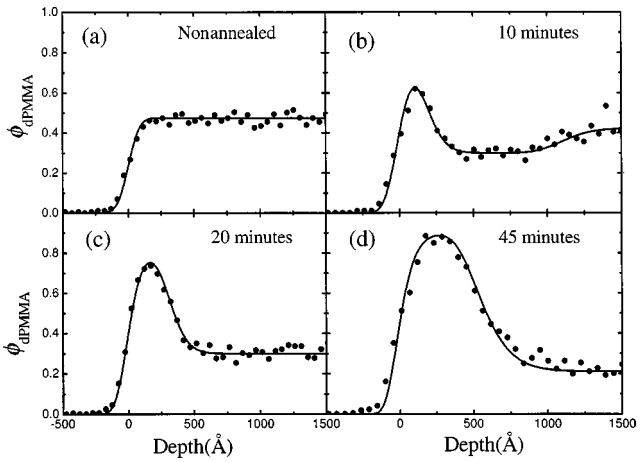

FIG. 1. The dPMMA depth profile for a dPMMA:SAN blend annealed at 190 °C determined by LE-FRES. (a) The as-cast sample has a uniform dPMMA volume fraction of 0.47. (b) After 10 min, the surface forms a dPMMA-rich layer around 150 Å. The adjacent layer is depleted of dPMMA and contains an excess of SAN. (c) and (d) show that the wetting layer thickness increases from 260 to 520 Å after 20 and 45 min, respectively. The solid lines are least square fits to the spectra using step volume fraction profiles convoluted with the experimental resolution, a Gaussian function with a FWHM of 160 Å.

The surface roughness and near surface morphology were determined at room temperature using a Digital Instrument Dimension 3000 atomic force microscope (AFM). Because the glass transition temperatures of dPMMA and SAN are 105 °C and 115 °C, respectively, the morphology was preserved after quenching from 185 °C to room temperature. By exposing samples to acetic acid for 2 min, the *A*-rich wetting layer and internal phase was selectively removed leaving only the nonwetting *B*-rich phase. To demonstrate that wet etching did not change morphology, AFM images of the same sample after 2 min and 60 min in acetic acid were taken and found to be identical. Because ion radiation crosslinks B, ion-bombardment was used to help ''fix'' the *B* morphology. The AFM images of *B* were all taken from ion beam treated samples. Control experiments showed that the ion beam exposure did not change feature size or shape. The AFM measurements were obtained in tapping mode using a SiO_2 tip. The driving frequency and amplitude were 278.566 kHz and 428 mV, respectively. A scan rate of 0.8 Hz was used to image a lateral area of 10 μm$\times$10 μm.

III. RESULTS AND DISCUSSION

Upon annealing at 190 °C, Fig. 1 shows how the near-surface volume fraction of *A* in *AB* film increases with time during the second stage of phase separation. Initially, the *A* volume fraction of 0.47 is uniformly distributed throughout the film. Figure 1(a) shows that the near-surface region contains a homogeneous distribution of *A*, consistent with an equilibrium starting state. After 10 min, the surface is enriched by the *A*-rich phase whereas the adjacent region (30 to 80 nm) is depleted of A as shown in Fig. 1(b). The wetting layer thickness l is determined from a step profile having a pure *A* wetting layer followed by an *AB* blend. The solid

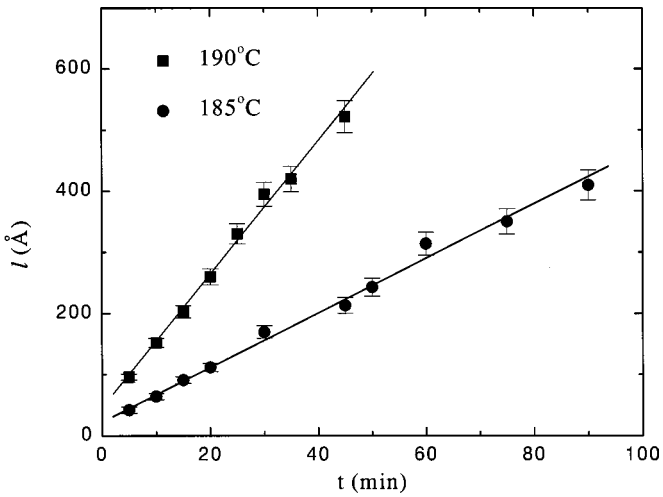

FIG. 2. Wetting layer thickness as a function of annealing time at 185 °C (solid circles) and 190 °C (solid squares). The solid lines are least square fits showing that l varies linearly with t. The growth rate dl/dt at 190 °C is 1.82 times that at 185 °C, which is consistent with a temperature dependence determined by $\sigma(T)/\eta(T)$.

lines in Fig. 1 represent step profiles convoluted with the instrumental resolution. As shown in Figs. 1(b), 1(c) and 1(d), l increases from 150 to 260 Å, and to 520 Å as annealing time increases from 10 to 20 min, and to 45 min, respectively. Note that in the depletion layer the A volume fraction decreases from around 0.30 to around 0.20 between 10 and 45 min, respectively. This observation is consistent with the transport of A towards the surface. Correspondingly, the width of the depletion zone is expected to increase as demonstrated by comparing Figs. 1(b) and 1(c). Because it laterally averages over around 3 mm^2, LE-FRES is unable to distinguish between a homogeneous and two-phase mixture within the depletion layer. In the former case, wetting layer growth is expected to be diffusion controlled and increase as $t^{1/3}$. In the latter case, bicontinuous tubes in the bulk can provide a pathway for hydrodynamic flow of A to the surface resulting in a much faster wetting layer growth.

Figure 2 shows that the wetting layer thickness increases linearly with time at 185 °C (solid circles) and 190 °C (solid squares). Near the end of this stage, the wetting layer thickness reaches around 400 Å and 500 Å at 185 and 190 °C, respectively. For both temperatures, l appears to approach a finite value at $t=0$, suggesting that wetting occurs very rapidly between 0 and 2 min. In Fig. 2, the slopes provide a measure of the growth rate, $r=dl/dt$. The ratio of the growth rates is $r_{190\,^\circ\mathrm{C}}/r_{185\,^\circ\mathrm{C}}=1.82$. This data provides convincing evidence that the surface wetting layer can grow as t^1 in critical polymer blends. This observation is consistent with a hydrodynamic-flow transport mechanism. To complement the studies of wetting layer growth, direct evaluation of the depletion layer morphology is needed

The depletion layer morphology determines how the wetting component is transported from the bulk to the surface. Using a Ginzburg-Landau bulk free-energy with a long-range surface interaction, Chen and Chakrabarti [17] demonstrated that diffusion limited wetting is characterized by a contiguous depletion layer whereas hydrodynamic-flow-driven wetting occurs when the depletion layer contains perforations. Using AFM, Fig. 3 shows the surface roughness

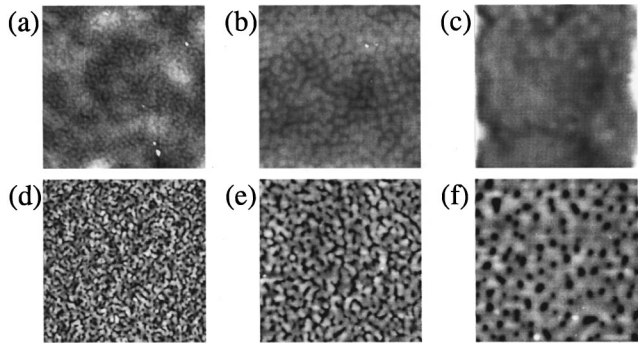

FIG. 3. AFM images of samples before (top row) and after (bottom row) selective etching of dPMMA. Samples were annealed at 185°C for 20 min [(a) and (d)], 60 min [(b) and (e)], and 120 min [(c) and (f)]. High and low regions are light and dark, respectively. (a)–(c) show that the surface roughness increases with time. The depletion layer is characterized by a bicontinuous, phase-separated morphology [(d) and (e)] during the second regime of growth. The dimensions of the nonwetting phase are in excellent agreement with the surface hills in (a) and (b). Eventually, the bicontinuous morphology coarsens resulting in an SAN rich continuous phase (light) perforated with dPMMA-rich cylinders (dark) as shown in Fig. 3(f). All the images are 10 μm$\times$10 μm.

(top row) and the morphology of the nonwet phase (bottom row) after 20 min (left column), 60 min (middle column), and 120 min (right column) at 185 °C. The high (light) and low (dark) regions reflect the increase in surface roughness [Figs 3(a), 3(b), and 3(c)] and lateral size of the nonwetting B phase [Figs. 3(d), 3(e), and 3(f)]. Figures 3(a)–3(c) show that the hills are uniformly distributed across the surface and grow higher and wider. Correspondingly, the root mean square roughness increases from 2.36 to 3.86 nm to 5.25 nm, respectively. For reference, the roughness of the as-cast sample is only 0.55 nm. Note that the hill diameter increases whereas the number density decreases with time. Because the A component has been removed, Figs. 3(d), 3(e) and 3(f) reflect the B morphology in the near-surface region. Figures 3(d), and 3(e) show that a bicontinuous phase morphology, characteristic of spinodal decomposition, forms during this second stage. These images provide direct evidence for A-rich channels (dark) within the depletion layer. These channels bridge the surface phase and the bulk and serve as pathways for hydrodynamic flow. As expected, the channel width increases between 20 min and 60 min. A detailed analysis of channel coarsening will be presented at a later time. As shown in Fig. 3(f), after 120 min, the bicontinuous morphology has evolved into a membranelike, continuous B-rich phase (light) perforated with A-rich domains (dark). This morphology is characteristic of the third stage of wetting and phase separation in these thin film blends.

To accentuate the A-rich channels shown in Fig. 3(e), a surface plot of the same image is presented in Fig. 4. In this figure, the connectivity of the nonwetting B-rich phase is more clearly illustrated. By taking a fast Fourier transform, the characteristic wave vector q_m is found to be 7.23×10^{-3} nm^{-1}. Because the lateral correlation length $2\pi/q_m=869$ nm is greater than the film thickness of 495 nm, the symmetry of domain growth is broken. Figure 2 shows that the wetting layer growth rate is unperturbed by the asymmetric internal phase growth.

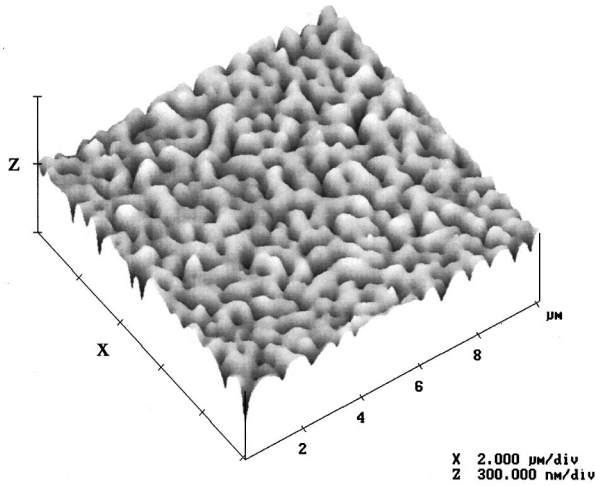

FIG. 4. An AFM prospective plot of the sample shown in Fig. 3(e) emphasizing the bicontinuous morphology of the SAN (light) and dPMMA (dark, removed). The characteristic length parallel to the surface is 869 nm. The direct observation of dPMMA channels in the depletion layer further supports the claim of hydrodynamic flow driven wetting in this system.

Taken together, depth and lateral profiles provide unambiguous evidence for both signatures of hydrodynamic-flow driven wetting, namely a wetting layer that grows as t^1 accompanied by channels between the wetting layer and bulk phase. The hydrodynamic driving force results from the interfacial curvature of the bicontinuous, phase-separated morphology, which produces a capillary pressure gradient towards the wetting layer [7]. This pressure gradient drives the bulk *A*-rich phase to the surface resulting in the hills observed in Figs. 3(a)–3(c). The curvature of the surface hill generates an inward capillary pressure to balance the internal pressure. Thus, the surface topography directly reflects the internal structure as originally proposed by Jandt *et al.* [11].

Assuming complete wetting and hydrodynamic flow, Tanaka [7,8] proposed that the wetting layer should grow as $l=k(\sigma/\eta)t$, where k,σ and η are a proportionality constant, the interfacial tension, and the viscosity of the wetting phase, respectively. This equation also assumed a late stage hydrodynamic phase coarsening mechanism [18,19]. Because polymer melts commonly have low σ and large η, polymer wetting layers generally grow much more slowly than in the case of liquids. The temperature dependence of the wetting layer growth is determined by $\sigma(T)/\eta(T)$. As T increases, σ increases whereas η decreases for our A:B blend. Thus, $\sigma(T)/\eta(T)$ (and therefore l) should increase strongly with T. From the data in Fig. 2, the growth rate increases by a factor of 1.82 as T increases by only 5 °C. Because the temperature dependence of σ is relatively small, $\eta(T)$ is expected to dominate the growth rate temperature dependence. From the PMMA viscosity [20], the ratio $\eta(185\,^\circ\mathrm{C})/\eta(190\,^\circ\mathrm{C})$ is 1.89, in excellent agreement with experimental results.

Recent polymer studies [4,5] have mainly focused on wetting behavior of thick films in order to avoid complications arising from confinement effects. In these studies the coarsening of the surface phase was measured after the formation of a surface directed oscillatory profile. For critical compositions, the nonwetting phase is thought to form a continuous layer and therefore diffusion of the wetting component from the bulk to the surface limits the wetting layer growth. As expected for diffusion controlled domain growth, the wetting layer was found to grow as $t^{1/3}$ [4,5]. The main difference between these critical blend studies and this paper is that thin film confinement prevents the formation of a contiguous depletion layer in our studies [16]. To allow for hydrodynamic flow, transport of the wetting component from the bulk to the surface must take place via channels in the depletion layer. This pathway can be established in an off-critical blend where the majority component wets the surface or via thinning of the depletion layer adjacent to the wetting layer [5,11]. However, we propose that the interference of the coarsening composition profiles originating from the surface and substrate prevents a continuous depletion layer from forming. This interference was previously observed by Krausch *et al.* [21].

The evidence for hydrodynamic flow driven wetting in polymer blends is limited. In an off-critical isotopic blend where the majority component wets the surface, Krausch *et al.* [5] reported that the wetting layer grew as t^1 in agreement with hydrodynamic flow. These studies were based on a limited range of data and relied on morphology inferred from computer simulations. Jandt *et al.* [11] observed transient surface roughening in thin films which they attributed to hydrodynamic flow through perforations in the nonwetting phase. However, the internal morphology was not reported. In contrast, by measuring the wetting layer growth rate, surface roughness and internal morphology in *AB* blend, a rigorous test of hydrodynamic flow driven wetting in polymer blends has been observed.

IV. SUMMARY

In this paper we report two signatures of hydrodynamic flow driven wetting in phase separating thin film *AB* blends at the critical composition. Using LE-FRES, the thickness of *A* wetting layer is observed to grow linearly with time at 185 °C and 190 °C. AFM was used to show an increase in surface roughness with time, consistent with *A* transport by hydrodynamic flow through perforations in the depletion layer. By selective etching of the *A*-rich phase, the internal morphology is revealed and shown to form a bicontinuous interconnected morphology. The t^1 wetting layer growth rate and *A*-rich channels bridging the bulk and the surface layer are consistent with a hydrodynamic-flow-driven wetting mechanism.

ACKNOWLEDGMENTS

We acknowledge primary financial support from NSF DMR program, Grant Nos. DMR95-26357 and DMR-9974366. The ion beam and AFM studies were supported by the NSF MRSEC program, Grant No. DMR96-32598. We acknowledge stimulating discussions with Dr. Charles C. Han.

[1] S. Dietrich, in *Phase Transition and Critical Phenomena*, edited by C. Domb and J. L. Lebowitz (Academic Press, London (1988), Vol. 12.
[2] *Modern Approaches to Wettability: Theory and Applications*, edited by M. E. Schrader and G. I. Loeb (Plenum Press, New York, 1992).
[3] L. A. Utracki, *Polymer Alloys and Blends* (Hanser, New York, 1989).
[4] G. Krausch, C. Dai, E.J. Kramer, and F.K. Bates, Phys. Rev. Lett. **71**, 3669 (1993).
[5] G. Krausch, E.J. Kramer, F.K. Bates, J.F. Marko, G. Brown, and A. Chakrabarti, Macromolecules **27**, 6768 (1994).
[6] W. Straub, F. Bruder, R. Brenn, G. Krausch, H. Bielefeldt, A. Kirsch, O. Marti, J. Mlynek, and F. Marko, Europhys. Lett. **29**, 353 (1995).
[7] H. Tanaka, Phys. Rev. Lett. **70**, 2770 (1993).
[8] H. Tanaka, Phys. Rev. E **54**, 1709 (1996).
[9] P. Wiltzius and A. Cumming, Phys. Rev. Lett. **66**, 3000 (1991); A. Cumming, P. Wiltzius, F.S. Bates, and J.H. Rosedale, Phys. Rev. A **45**, 885 (1992).
[10] R.A.L. Jones, L.J. Norton, E.J. Kramer, F.S. Bates, and P. Wiltzius, Phys. Rev. Lett. **66**, 1326 (1991).
[11] K.D. Jandt, J. Heier, F.S. Bates, and E. Kramer, Langmuir **12**, 3716 (1996); J. Heier, E. Kramer, P. Revesz, G. Battistig, and F.S. Bates, Mater. Charact. **32**, 3758 (1999).
[12] P. Guenoun, D. Beysens, and M. Robert, Phys. Rev. Lett. **65**, 2406 (1990); Physica A **172**, 137 (1991).
[13] H. Wang, B. Zhang Newby, and R. J. Composto (unpublished).
[14] The thickness of the oxide layer is measured using neutron reflectivity.
[15] J. Genzer, J.B. Rothman, and R.J. Composto, Nucl. Instrum. Methods Phys. Res. B **86**, 345 (1994).
[16] H. Wang, Ph.D. thesis, University of Pennsylvania, 1999 (unpublished).
[17] H. Chen and A. Chakrabarti, Phys. Rev. E **55**, 5680 (1997).
[18] S.M. Troian, Phys. Rev. Lett. **71**, 1399 (1993).
[19] E.D. Siggia, Phys. Rev. A **20**, 595 (1979).
[20] S. Wu, J. Polym. Sci., Part B: Polym. Phys. **25**, 2511 (1987).
[21] G. Krausch, C. Dai, E.J. Kramer, J.F. Marko, and F.K. Bates, Macromolecules **26**, 5566 (1993).